ISSN (ONLINE): 2454-9762
ISSN (PRINT): 2454-9762

International Journal of Advanced Research in Management, Architecture, Technology and Engineering (IJARMATE)
Vol. 2, Issue 10, October 2016

Liver And Tumor Segmentation Using Massive Training Artificial Neural Network

Christo Ananth[1], Prof.R.S.Jha[2]

Research Scholar, Department of Electronics & Communication Engineering,
Calorx Teachers' University, Ahmedabad, Gujarat, India[1]
B.M.College of Technology and Management, Gurgaon, India[2]

***Abstract*— Adaptive initialization method allows a fully automatic liver and tumors segmentation employing active contour or graph-cut based techniques. MATLAB 7.11.0 (R 2010b) tool is used to implement this proposed work. This study presented the implementation of two fully automatic liver and tumors segmentation techniques and their comparative assessment. Image segmentation plays a crucial role in many medical-imaging applications, by automating or facilitating the delineation of anatomical structures and other regions of interest. Many methods are existing and still developing the new methods for the segmentation to overcome the shortcomings of the existing methods. The liver image is segmented by using GC-OAAM approach in Phase I. This segmentation work is analyzed by using confusion algorithm. The performance is improved by the implementation of multiple MTANN. The MTANN supervised filter was effective for enhancement in medical images and is useful for improving the sensitivity and specificity. The described adaptive initialization method enabled fully automatic liver surface segmentation with both Geodesic Graph Cut and Graph-Cut techniques, demonstrating the feasibility of two different approaches. The comparative assessment showed that the Geodesic Graph-cut method provided superior results in terms of accuracy and did not present the described main limitations related to the Graph Cut method. In the previous work, the initialization technique was applied to Graph Cuts algorithm demonstrating the robustness and effectiveness of automatic liver segmentation.**

In this study, the initialization method was further extended to Geodesic Graph cut algorithm in order to enable full automation of this method and evaluate potential improvements with respect to previous automatic presented approaches and then to the ground truth. The same segmentation approaches were then applied also to segmentation of liver tumors. Even if there are some theoretical connections between discrete geometry of Geodesic Graph-cuts and integral and differential geometry related to Graph Cuts approach, important differences cannot be neglected for algorithm implementations and comparative assessment of the results.

***Index Terms*— Graph-cut method, Geodesic Graph Cut method, Active Contours model, Live Wire method, Active Appearance model, Massive Training Artificial Neural Network.**

I. INTRODUCTION

There are number of techniques to segment an image into regions that are homogeneous. The development of these imaging technologies is the first step towards improvement of diagnosis accuracy and patient quality of life. Liver extraction from hepatic CT images is challenging because the liver often abuts other organs of a similar density. Computed Tomography (CT) is probably the most widely adopted medical image technology build on X-rays transmission, that allows through image processing techniques to get 2-D cross-section images and then, from a stack of 2-D slices, a 3-D organ reconstruction. Computed tomography (CT) and magnetic resonance imaging (MRI) have been identified as accurate non-invasive imaging modalities in the diagnosis of the liver cancer. These medical images are interpreted by radiologists. However, image interpretation by human beings is often limited due to the non-systematic search patterns of themselves, the presence of structural noise in the image, and the presentation of complex disease states requiring the integration of vast amount of image data and clinical information. As the liver can stretch across well over 150 slices in a CT image and contain up to dozens of lesions, manual segmentation is tedious and prohibitively time consuming for a clinical setting. There are many approaches for image segmentation, such as feature thresholding, contour based techniques, region based techniques, clustering, and template matching. Each of these approaches has its advantages and disadvantages in terms of applicability, suitability, performance, and computational cost. Particularly, no one who did not consider above characteristics of the abdominal CT image can meet desirable results on liver segmentation. In addition, the traditional method of getting volume of the liver is to perform a by-hand 2D segmentation of parallel cross-sectional CT slices and to multiply all voxels of the stacked slices by their size while the procedure is often time consuming and non-systematic. Image segmentation is often described as the process of separating an image into regions of interest–object and background–usually guided by regional statistics involving image values.

However, sometimes directly computing such statistics on image values is not enough to discriminate regions. In a number of important cases, the image may be transformed into a more information rich form to yield latent discriminating features. Image segmentation consists of

ISSN (ONLINE): 2454-9762
ISSN (PRINT): 2454-9762

International Journal of Advanced Research in Management, Architecture, Technology and Engineering (IJARMATE)
Vol. 2, Issue 10, October 2016

separating an image into different regions and is one of the most widely studied problems in image processing. There are three main segmentation categories: fully automatic methods, semi-automatic methods, and (almost) completely manual ones. The framework here proposed falls in the semi-automatic category.

In particular, the segmentation is obtained after the user has provided rough scribbles labeling the regions of interests. This type of user intervention can help to segment particularly difficult images. Moreover, it is often imperative to mark the regions of interest, which completely depend on the user and the application. For example, the user might be interested in separating a selected object (foreground) from the rest of the image (background), independently of how complicated this background is. A number of very inspiring and pioneering user-assisted segmentation type algorithms of the style were used for image segmentation. In many cases, the tissues or organ of interest is difficult to be separated from its surroundings, when they share similar intensity levels. With the other tissues, and their boundaries lack strong edge information. For example, CT technique is weak at imaging soft tissues. It cannot differentiate grey and White matters well in neural tissues.

Besides of the image information, higher level knowledge of anatomy and pathology is critical for medical image segmentation. Usually medical image has complex appearance due to the complicated anatomic structures. Medical expertise is required to understand and interpret the image, so that the segmentation algorithms could meet the clinician's needs. Segmentation results should always be validated by clinicians as well.

The Level-set method proposed for cartoon colorization initializes a curve at the user-provided scribble and evolves it until it finds boundaries of the region of interest. The speed of the moving front depends on local features and global properties of the image. Segmentation algorithm was presented based on the assumption that if a pixel is a linear combination of its neighbors, then its label will be the same linear combination of its neighbors' labels. The segmentation of natural images and videos is one of the most fundamental and challenging problems in image processing. One of its applications is to extract the foreground object (or object of interest) out of the cluttered background, and, for example composite it onto a new background without visual artifacts.

For complex images, as well as subjective applications, there can be more than one interpretation of the foreground or objects of interest (in absence of higher level knowledge), thus making the task ill-posed and ambiguous. It is often imperative then to incorporate some user intervention, which encodes prior information, into the process. Specifically, the user can draw rough scribbles labeling the regions of interest and then the image/video is automatically segmented. The user is allowed to add more scribbles to achieve the ideal result, although of course, the goal is to minimize as much as possible the user effort. Closely connected to the segmentation of objects of interest, image and video matting refers to the process of reconstructing the foreground/background components and the alpha value (transparency) of each pixel. This is important for applications such as extracting hair strands or blurry edges, as well as for compositing.

Image segmentation has often been defined as the problem of localizing regions of an image relative to content (e.g., image homogeneity). However, recent image segmentation approaches have provided interactive methods that implicitly define the segmentation problem relative to a particular task of content localization. This approach to image segmentation requires user (or preprocessor) guidance of the segmentation algorithm to define the desired content to be extracted. A practical interactive segmentation algorithm must provide four qualities: 1) Fast computation, 2) Fast editing, 3) An ability to produce an arbitrary segmentation with enough interaction, 4) Intuitive segmentations. Algorithms generally require the solution of a sparse, symmetric positive-definite system of linear equations which may be solved quickly through a variety of methods. The algorithm may perform fast editing by using the previous solution as the initialization of an iterative matrix solver. An arbitrary segmentation may also be achieved through enough user interaction.

Supervised segmentation algorithms typically operate under one of two paradigms for guidance: 1) Specification of pieces of the boundary of the desired object or a nearby complete boundary that evolves to the desired boundary, 2) Specification of a small set of pixels belonging to the desired object and (possibly) a set of pixels belonging to the background. Any of the automatic segmentation algorithms might be considered supervised by subsequent user selection of the desired segment. However, if the desired object is not a complete segment, a secondary clustering/segmentation algorithm must be employed to split or merge the automatic segments. The intelligent scissors algorithm treats the image as a graph where each pixel is associated with a node and a connectivity structure is imposed. This technique requires the user to place points along the boundary of the desired object. Supervised Segmentation algorithms naturally produce satisfactory results to image segmentation. The watershed of a function (seen as a topographical surface) is composed of the locations from which a drop of water could flow towards different minima. The framework allowing the formalization and proof of this statement is the optimal spanning forests relative to the minima. For the purpose of seeded image segmentation, the gradient of the image can be considered as a relief map and, instead of minima, seeds may be placed by the user or found automatically to specify the segmentation of the image into desired regions. A maximum (minimum) spanning forest (MSF) algorithm computes trees spanning all the nodes of the graph, each tree being connected to exactly one connected seed component, and the weight of the set of trees being maximum (minimum).An optimal spanning forest can be computed with an algorithm in quasi-linear time. Watersheds are widely used in image segmentation because there exist numerous and efficient algorithms that are easy to implement. However, segmentation results from watersheds may suffer from leaks and degeneracy of the solution on the plateaus of the weight function.

ISSN (ONLINE): 2454-9762
ISSN (PRINT): 2454-9762

International Journal of Advanced Research in Management, Architecture, Technology and Engineering (IJARMATE)
Vol. 2, Issue 10, October 2016

The labeling produced by the graph cuts (GC) algorithm is determined by finding the minimum cut between the foreground and background seeds via a maximum flow computation. The original work on GC for interactive image segmentation has been subsequently extended by several groups to employ different features or user interfaces. Although GC is relatively new, the use of minimal surfaces in segmentation has been a common theme in computer vision for a long time and other boundary based user interfaces have been previously employed. Two concerns in the literature about the original GC algorithm are metrication error ("blockiness") and the shrinking bias. Metrication error was addressed in subsequent work on GC by including additional edges, by using continuous max flows or total variation. These methods for addressing metrication error successfully overcome the problem, but may incur greater memory and computation time costs than the application of maximum flow on a 4-connected lattice. The shrinking bias can cause overly small object segments because GC minimizes boundary length. Although some techniques have been proposed for addressing the shrinking bias, these techniques all require additional parameters or computation.

The random walker (RW) algorithm is also formulated on a weighted graph and determines labels for the unseeded nodes by assigning the pixel to the seed for which it is most likely to send a random walker. This algorithm may also be interpreted as assigning the unlabeled pixels to the seeds for which there is a minimum diffusion distance, as a semi-supervised transduction learning algorithm or as an interactive version of normalized cuts. Additionally, popular image matting algorithms based on quadratic minimization with the Laplacian matrix may be interpreted as employing the same approach for grouping pixels, albeit with different strategies to determine the edge weighting function. Diffusion distances avoid segmentation leaking and the shrinking bias, but the segmentation boundary may be more strongly affected by seed location than with graph cuts.

The shortest path algorithm assigns each pixel to the foreground label if there is a shorter path from that pixel to a foreground seed than to any background seed, where paths are weighted by image content in the same manner as with the GC and RW approaches. This approach was recently popularized but variants of this idea have appeared in other sources. The primary advantage of this algorithm is speed and prevention of a shrinking bias. However, it exhibits stronger dependence on the seed locations than the RW approach, is more likely to leak through weak boundaries (since a single good path is sufficient for connectivity) and exhibits metrication artifacts on a 4-connected lattice. All of the above models may be considered as addressing energies comprised of only unary and pairwise (binary) energy terms. However, recent literature has found that the addition of energy terms defined on higher-order cliques can help improve performance on a variety of tasks. Although higher-order cliques are not addressed, an equivalent construction of pair wise terms has seen recent progress. Despite the recent popularity of energies defined on higher order cliques, pair wise terms (and watersheds) are still used in the computer vision literature and any improvement to these models can have a broad impact.

Regularization is of central importance to image segmentation and inpainting. The introduction of higher-order regularizers in respective energy minimization approaches is known to give rise to substantial computational challenges. Some of the most powerful approaches to image segmentation are based on region integrals with regularity terms defined on the region boundaries. While many such methods make use of length as a regularity term, only few use curvature regularity. This is in contrast to psychophysical experiments on contour completion where curvature was identified as a vital part of human perception.
Length regularization has become an established paradigm because there exist many powerful algorithms for computing optimal solutions for length-regularized energies, either using discrete graph-theoretic approaches based on the min-cut/max-flow duality or using continuous PDE-based approaches using convex relaxation and thresholding theorems.

The modern variations on interactive segmentation algorithms are primarily built on top of a small set of core algorithms — graph cuts, random walker and shortest paths, which are reviewed shortly. Recently these three algorithms were all placed into a common framework that allows them to be seen as instances of a more general seeded segmentation algorithm with different choices of a parameter q.

II. MATERIALS AND METHODS

The Existing System used Automatic and Semiautomatic methods for Liver segmentation which provides manual delineations of liver contours and tumors on diagnostic images. But it consumes more time and it produces intrinsic low reproducibility. 2 Main Approaches were mainly involved. They are Intensity-based & Model-based methods. Intensity-based method is based on Thresholding and Morphological filtering. Model-based approach is based on active contours model. But here there is no proper setting of processing steps & modality and it requires manual initialization based on learning database or on user interfaces. The Existing system used Interactive image segmentation via adaptive weighted distances which do not explicitly consider and accurately localize object boundaries. Moreover the Curvature regularity method provides curvature-minimizing technique to smooth boundaries. But it does not use an edge component to localize edges and it consumes more time. In the previous work, Graph-cut approach was used which is explicitly used in edge-finding and used as region-modeling components. In this proposed method, same segmentation method for liver was applied and for its internal pathological structures.The technique produces improved segmentation than earlier methods and it was a good Energy minimization algorithm. But the approach was not applicable to large systems and this approach was not fast and effective.

1. Xinjian Chen, Jayaram K. Udupa, Ulas Bagci, Ying Zhuge, and Jianhua Ya, "Medical Image Segmentation by Combining Graph Cuts and Oriented Active Appearance

ISSN (ONLINE): 2454-9762
ISSN (PRINT): 2454-9762

International Journal of Advanced Research in Management, Architecture, Technology and Engineering (IJARMATE)
Vol. 2, Issue 10, October 2016

Models", in proc. IEEE Transactions On Image Processing, Vol. 21, No. 4, April 2012.

In this paper, a novel method based on a strategic combination of the active appearance model (AAM), live wire (LW), and graph cuts (GCs) for abdominal 3-D organ Segmentation is proposed. The proposed method consists of three main parts: model building, object recognition, and delineation. In the model building part, we construct the AAM and train the LW cost function and GC parameters. In the recognition part, a novel algorithm is proposed for improving the conventional AAM matching method, which effectively combines the AAM and LW methods, resulting in the oriented AAM (OAAM). A pseudo-3-D initialization strategy is employed and segmented the organs slice by slice via a OAAM method. For the object delineation part, a 3-D shape-constrained GC method is proposed. The object shape generated from the initialization step is integrated into the GC cost computation, and an iterative GC–OAAM method is used for object delineation. The proposed method was segmenting the liver, kidneys, and spleen in an abdomen.

In [1],The main goals of segmentation are to be (i) to provide effective control to the user, and (ii) to minimize the total user's time required in the process. In this paper, authors have proposed two paradigms, referred to as live wire and live lane. In live wire, the user first selects an initial point on the boundary. An optimal path from the initial point to the current point is found and displayed in real time. The user thus has a live wire on hand which is moved by moving the cursor. If the cursor goes close to the boundary, the live wire snaps onto the boundary. In live lane, the user selects only the initial point. Subsequent points are selected automatically as the cursor is moved within a lane surrounding the boundary whose width changes as a function of the speed and acceleration of cursor motion. Live-wire segments are generated and displayed in real time between successive points. This method is1.5–2.5 times faster than manual tracing.

In [2], the authors have proposed a segmentation method based on Markov random fields, which combined shape priors and regional statistics. To encode the image support, a Voronoi decomposition of the domain is considered and regional based statistics are used. The resulting model is computationally efficient, can encode complex statistical models of shape variations. The main challenges of knowledge-based segmentation are: (i) appropriate modeling of shape variations, (ii) successful inference between the image and the manifold. In this knowledge based approach, defined the shape model as an incomplete graph. The proposed approach aims to optimize the connectivity of the graph nodes, and learns the structure and the local deformation statistics of an object from a set of training examples. However, this method did not perform segmentation at the pixel level.

In [3], the authors devise a graph cut algorithm for interactive segmentation which incorporates shape priors. Interactive or semi-automatic segmentation is a useful alternative to pure automatic segmentation in many applications the graph cuts approach guarantees a global optimum. The related work falls into two categories: segmentation using shape priors, and globally optimal methods for segmentation. The shape priors are embedded into the weights on the edges in the graph, by using a level-set formulation. Transformations of the shape template are also taken into account. The main direction for future research is to examine whether more complex transformations of the template can be easily incorporated into the scheme.

In [4], the proposed algorithm utilizes the shape model of the target organ to gain robustness in the case where the objective organ is surrounded by other organs or tissue with the similar intensity profile. The algorithm labels the image based on the graph-cuts technique and incorporates the shape prior using a technique based on level-sets. The method requires proper registration of the shape template for an accurate segmentation, so propose a unified registration-segmentation framework to solve this problem. In order to reduce the computational cost of the minimization step, the proposed segmentation algorithm operates on homogeneous regions instead of voxels. The algorithm, operating on a properly registered template, captures the boundary of the object, even if it is diffuse or weak. The registration algorithm uses the segmentation energy as a measure of how well the template is fit to the input image, and minimizes that energy over the space of transformations. In this way, the proposed algorithm registers the template and segments the image simultaneously.

In [5], a probabilistic method for segmenting instances of a particular object category within an image is explained. This approach overcomes the deficiencies of previous segmentation techniques based on traditional grid conditional random fields (CRF), namely that 1) they require the user to provide seed pixels for the foreground and the background and 2) they provide a poor prior for specific shapes due to the small neighborhood size of grid CRF. Automatically obtain the pose of the object in a given image instead of relying on manual interaction. This "objcut" method include: 1) efficient algorithms for sampling the object category models and 2) the observation that a sampling-based approximation of the expected log-likelihood of the model can be increased by a single graph cut. This method efficiently provides accurate segmentation which resembles the object. The accuracy of the segmentation can be attributed to the novel probabilistic model.

In [6], an accurate and efficient segmentation is achieved by incorporating Bayesian nonlinear shape priors into an iterative graph cut methods. Using kernel principle component analysis, demonstrate how a shape projection pre-image can induce an iteratively refined shape prior in a Bayesian manner. From a user-initialized segmentation, the algorithm proceeds iteratively. The shape model is learned from a set of training examples via PCA and the shape prior generated by pre-image projection. Taking advantage of efficient algorithms for global min-cut solutions, cast the energy-based image segmentation problem in a graph structure of which the min-cut corresponds to a globally optimal segmentation. In this paper, the author has not

ISSN (ONLINE): 2454-9762
ISSN (PRINT): 2454-9762

International Journal of Advanced Research in Management, Architecture, Technology and Engineering (IJARMATE)
Vol. 2, Issue 10, October 2016

explored that the segmentation of multiple objects with the multi label graph cut algorithm.

In [7], the authors present a new shape prior segmentation method using graph cuts capable of segmenting multiple objects. The shape prior energy is based on a shape distance popular with level set approaches and incorporate this energy into the graph via terminal edge weights. Also present a multiphase graph cut framework to simultaneously segment multiple, possibly overlapping objects. The multiphase formulation differs from multi way cuts in that the former can account for object overlaps by allowing a pixel to have multiple labels. A major advantage of our framework over variational methods is that it explicitly minimizes the segmentation energy and thereby avoids the computation of the energy gradient, which can be difficult and often requires approximations. The results show that the algorithm is insensitive to initializations and noise and is efficient in practice.

In [8], the author describes a method for automatic recognition of abdominal organs such as kidneys, spleen, stomach, and liver from computing tomography (CT) images using three-dimensional (3D) mathematical morphology. Morphological approaches provide the theory and tools to analyze shapes directly. This characteristic enables analyzing and recognizing abdominal organs according to size and gray level features. First, identify the coordinate origin and the scale in the abdominal region and then set up four regions for recognition. The recognition process consists of two steps: segmentation and identification. For the segmentation step, employ a differential top-hat (DTT) operation. For the identification step, first identify the vertebra that the lowest rib meets. In three regions, we separate organs based on threshold values, while in a region containing the liver and stomach use RE (Recursive Erosion) and GI (Geodesic Influence) in order to separate touched organs. The separated organs are identified or labeled based on the size and position. From this method is obtained a recognition rate of about 91% for nine organs of four CT images.

In [9], a fully automatic method for liver segmentation on contrast-enhanced CT images is proposed. This method delineates the skin, bones, lungs, kidneys and spleen, by combining the use of thresholding, mathematical morphology and distance maps then the liver is extracted. The method consists of the following main steps. First a seed region is determined that involves voxels which are located inside the liver. Then, the liver is separated from the heart to prevent over-segmentation in this region. Starting from the seed region the liver is segmented using an advanced region-growing (RG) method. When the CT image to be segmented is enhanced using some contrast agent, the abdominal organs can be easier separated due to different contrast intake of the different organs, which can be exploited when the region of the liver is automatically determined. This method can efficiently segment the liver parenchyma in many cases, however, in some cases the result may exclude very large lesions.

In [10], the author described about model-based segmentation. Model-based vision is a robust approach to recognizing and locating known rigid objects in the presence of noise, clutter, and occlusion. A model should only be able to deform in ways characteristic of the class of objects it represents. The key difference is that Active Shape Models can only deform to fit the data in ways consistent with the training set. This paper described Point Distribution Models (PDMs)-statistical models of shape. It represents an object as a set of labeled points, giving their mean positions and a small set of modes of variation. Active Shape Models exploit the linear formulation of PDMs, capable of rapidly locating the modeled structures in noisy, cluttered images-even if they are partially occluded.

III. METHODOLOGY

This paper mainly deals with the multiple Massive-Training Artificial Neural Network (MTANN) based segmentation techniques. The MTANN consists of a modified multilayer ANN, which is capable of operating on image data directly. The MTANN is trained by use of a large number of sub-regions extracted from input images together with the teacher images These MTANN based segmentation techniques involves training with massive sub-region-pixel pairs which is expected to give better results. Performance analysis of segmented images can be done both qualitatively and quantitatively.

In this method of analysis, segmented images are evaluated visually. But this method of analysis is subjective or depends on type of application. The result of qualitative analysis will be different for different evaluators. This is because each evaluator will have distinct standard for measuring the quality of segmentation. In this paper, an output image is applied with ground truth image by image fusion algorithm and then the proposed algorithm is applied to evaluate the segmentation methods qualitatively.

There are many techniques for quantitatively evaluating segmented images. These techniques can be classified into three different categories. They are

1. Analytic methods
2. Supervised evaluation methods
3. Unsupervised evaluation methods.

In analytic method segmentation algorithms are treated directly based on some measures like complexity. In supervised segmentation method, the result of segmentation is compared with standard reference image which is segmented manually. In unsupervised segmentation method, the segmentation results are evaluated by judging the quality of segmented image directly to some predefined criteria.

Edge detection is fundamental in computer vision and imaging processing, among which, object detection is one of the most direct goals. Image segmentation and its performance evaluation are very difficult but important problems in computer vision. A major challenge in segmentation evaluation comes from the fundamental conflict between generality and objectivity. For general-purpose segmentation, the ground truth and

ISSN (ONLINE): 2454-9762
ISSN (PRINT): 2454-9762

International Journal of Advanced Research in Management, Architecture, Technology and Engineering (IJARMATE)
Vol. 2, Issue 10, October 2016

segmentation accuracy may not be well defined, while embedding the evaluation in a specific application, the evaluation results may not be extensible to other applications.

With GC-OAAM approach, the object (liver image) is detected or recognized from an abdominal organ. The liver image is recognized or initialized by boundary line detection using live wire and graph cut. This process is evaluated by image fusion. Using confusion matrix, the GC-OAAM segmented output is fused with ground truth image. Then the statistical measures are plotted as graph. The performance of the segmentation method is evaluated on the basis of important statistical measures such as, sensitivity, specificity, Matthews Correlation Co-efficient (MCC), Positive Predictive Value (PPV), Accuracy (ACC), True Positive (TP), False Positive (FP), True Negative (TN), and False Negative (FN). This performance graph is shown in Chapter 4. Now, let see the definition of statistical measures one by one.

Imagine a study evaluating a new test that screens people for a disease. Each person taking the test either has or does not have the disease. The test outcome can be positive (predicting that the person has the disease) or negative (predicting that the person does not have the disease). The test results for each subject may or may not match the subject's actual status. In that setting:

- True positive: Sick people correctly diagnosed as sick
- False positive: Healthy people incorrectly identified as sick
- True negative: Healthy people correctly identified as healthy
- False negative: Sick people incorrectly identified as healthy

In general, Positive = identified and negative = rejected. Therefore:

- True positive = correctly identified
- False positive = incorrectly identified
- True negative = correctly rejected
- False negative = incorrectly rejected

Sensitivity measures the proportion of actual positives which are correctly identified as such (e.g. the percentage of sick people who are correctly identified as having the condition). It is also called as true positive rate (TPR), or the recall rate in some fields.

Sensitivity relates to the test's ability to identify positive results. Sensitivity can be calculated using following formula.

$$\text{Sensitivity} = \frac{\text{No. of True Positives (TP)}}{\text{No. of True Positives (TP)} + \text{No. of False Negatives (FN)}} \text{ X100\%}$$

Sensitivity is not the same as the precision or positive predictive value (ratio of true positives to combined true and false positives), which is as much a statement about the proportion of actual positives in the population being tested as it is about the test.

Specificity measures the proportion of negatives which are correctly identified as such (e.g. the percentage of healthy people who are correctly identified as not having the condition). Sometimes it is also called as true negative rate. Specificity relates to the test's ability to identify negative results. Sensitivity can be calculated using following formula.

$$\text{Specificity} = \frac{\text{No. of True Negatives (TN)}}{\text{No. of True Negatives (TN)} + \text{No. of False Positives (FP)}} \text{ X 100\%}$$

Consider the example of the medical test used to identify a disease. The specificity of a test is defined as the proportion of patients that are known not to have the disease who will test negative for it. Specificity is also called as True Negative Rate (TNR).

The measure was introduced in 1975 by Matthews. The Matthews correlation coefficient is used in machine learning as a measure of the quality of binary (two-class) classifications. It takes into account true and false positives and negatives and is generally regarded as a balanced measure which can be used even if the classes are of very different sizes.

The MCC is in essence a correlation coefficient between the observed and predicted binary classifications; it returns a value between −1 and +1. A coefficient of +1 represents a perfect prediction, 0 no better than random prediction and −1 indicates total disagreement between prediction and observation. The statistic is also known as the phi coefficient.

While there is no perfect way of describing the confusion matrix of true and false positives and negatives by a single number, the Matthews correlation coefficient is generally regarded as being one of the best such measures. The MCC can be calculated directly from the confusion matrix using the formula:

$$MCC = \frac{(TP)(TN) - (FP)(FN)}{\sqrt{(TP+FP)(TN+FN)(TN+FP)(TN+FN)}}$$

In this equation, *TP* is the number of true positives, *TN* the number of true negatives, *FP* the number of false positives and *FN* the number of false negatives. If any of the four sums in the denominator is zero, the denominator can be arbitrarily set to one; this results in a Matthews correlation coefficient of zero, which can be shown to be the correct

ISSN (ONLINE): 2454-9762
ISSN (PRINT): 2454-9762

IJARMATE

International Journal of Advanced Research in Management, Architecture, Technology and Engineering (IJARMATE)
Vol. 2, Issue 10, October 2016

limiting value. The original formula which is in equation (3.3) is also equal to above was:

$$N = TP + FP + TN + FN$$

$$S = \frac{TP + FN}{N}$$

$$P = \frac{TP + FP}{N}$$

$$MCC = \frac{TP/N - S \times P}{\sqrt{PS(1-S)(1-P)}}$$

Matthews correlation coefficient is the geometric mean of the regression coefficients of the problem and its dual; the component regression coefficients of the Matthews correlation coefficient are markedness (deltap) and informedness (deltap').

Positive Predictive Value or precision is defined as the proportion of the true positives against all the positive results (both true positives and false positives).It is also denoted as PPV. It is equivalent to precision. The PPV of a measurement system, also called reproducibility or repeatability, is the degree to which repeated measurements under unchanged conditions show the same results. This is calculated by using the formula as:

$$PPV = \frac{TP}{TP + FP}$$

Positive Predictive Value or Precision is sometimes stratified into:

- Repeatability — the variation arising when all efforts are made to keep conditions constant by using the same instrument and operator, and repeating during a short time period.
- Reproducibility — the variation arising using the same measurement process among different instruments and operators, and over longer time periods.

Accuracy is the proximity of measurement results to the true value; precision, the repeatability, or reproducibility of the measurement. In the fields of science, engineering, industry, and statistics, the accuracy of a measurement system is the degree of closeness of measurements of a quantity to that quantity's actual (true) value.

The accuracy is the proportion of true results (both true positives and true negatives) in the population. It is a parameter of the test. Accuracy can be calculated as:

$$Accuracy = \frac{\text{No. of True Positives} + \text{No. of True Negatives}}{\text{No. of True Positives} + \text{False Positives} + \text{False Negatives} + \text{True Negative}}$$

Accuracy may be determined from Sensitivity and Specificity, provided Prevalence is known, using the equation:

Accuracy = (Sensitivity) X (Prevalence) + (Specificity) (1 - Prevalence)

A number of researchers have introduced a shape prior into a graph-cuts approach [6-8]. These papers show several ways to incorporate a general shape constraint, such as an ellipse, a star-shape, organ arbitrary shape defined by the user. A reference shape-based energy, computed by the Parzen window method [9] which is a population statistic based method but the combinatorial problem of multiple shape information re-mains unsolved. One proposed method [11] that combines the classification process with a graph-search algorithm but that method might fail in cases with large pathologies.

The paper in [10] combined a patient-specific shape, estimated by a statistical shape model (SSM), with a graph-cut to boost graph cut performance. It incorporated a prior knowledge about the region to be segmented based on neighbor structures (i.e. the dorsal ribs) and was shown to be effective in segmentation. However, the energy still suffered from low accuracy in lung segmentation as a result of the various patterns in shape, especially in the area close to the aorta However, all of the above methods consider single-shape information only, which might be different from the true shape, resulting in insufficient performance. Combining multiple-shape information will help to reduce such differences.

A graph cut formulates a segmentation problem as an energy minimization problem [6]. Given a set of voxels, P, and a set of labels, L= {0,1}, the goal is to assign a label l $\in$ L to each p $\in$ P. Let A_p denote a label assigned to voxel p, and let A= {A_1, A_2, ..., A_p, ..., $A_{|P|}$} be the collection of all label assignments. This gives the energy function:

$$E(A) = \lambda . R(A) + B(A) =$$

$$\lambda . \sum_{p \in P} \{ R_p (A_p) + + \sum_{\{p,q\} \in n} B_{p,q} . \delta A_p \neq A_q$$

There are two types of energy terms in Eq.(3.11). The first term is called the ‘‘data term’’, which expresses a penalty for

ISSN (ONLINE): 2454-9762
ISSN (PRINT): 2454-9762

International Journal of Advanced Research in Management, Architecture, Technology and Engineering (IJARMATE)
Vol. 2, Issue 10, October 2016

assigning label A_p to $voxel_p$. Generally, we use the negative log likelihood of the gray value for this term. The second term, $B_{p,q}$, is called the ''bound-ary term''. This term expresses a penalty for assigning labels A_p and A_q to the two neighboring voxels,p and q. This term originally relies on a gradient value between voxelspandq. The set Nis a collection of neighboring voxel pairs. The function δ is 1 if, $A_p \neq A_q$ and 0 otherwise. The coefficient λ in the equation is a constant value balancing the two terms.

One of the contributions of this paper is the proposal of an energy term that can penalize the segmentation boundary based on a human-specific shape. The following shape-constrained term, $S_{p,q}$, was introduced in the boundary term:

$$E(A) = \lambda . R(A) + B(A) =$$
$$\lambda . \sum_{p \in P} \{ R_p (A_p) + + \sum_{\{p,q\} \in n} B_{p,q}$$
$$. \delta A_p \neq A_q$$
$$S_{p,q} = \sqrt{\frac{1-\cos(\vartheta)}{2}})$$

where θ represents the angle between a vector connecting voxels p and q and a gradient vector of a signed distance φ(p) from the boundary of a given shape. Although the shape-constrained energy term $S_{p,q}$ has been shown to be effective, the algorithm still suffers from low accuracy, especially with test data. A patient-specific shape prior was estimated using an SSM beforehand. The estimation process works quite well for most cases, but it is still a challenging problem when dealing with test data in which an organ's shape is different from that found in a training dataset. Therefore, using only a single shape is risky. In this case, a collection of multiple shapes could ac-count for the shape in the test dataset.

A major contribution of this proposed graph-cuts-based segmentation algorithm that can consider multiple shapes. The proposed multi-shape graph cut-based segmentation algorithm improves liver segmentation by incorporating multiple shapes and prior information on neighbor structures. By permitting a graph cut algorithm to consider multiple shape priors, proposed method improves liver segmentation without relying too strongly on a single shape prior. Moreover, novel neighbor constrained energy terms is introduced to extract the liver with various shapes and appearances. Let see in detail later.

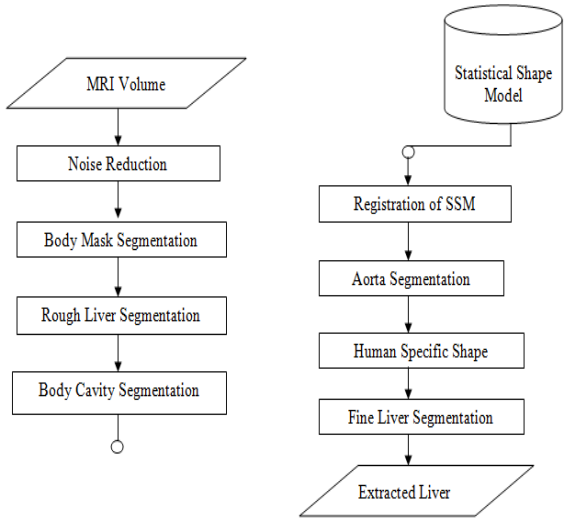

Fig.1. Flow Chart of the Multi-Shape Graph Cut Method

Fig.1. presents a flowchart of the liver segmentation system. The input to the system is a thoracic MRI volume and the first step is a noise reduction process based on median filtering (mask size: 333). Next, body mask segmentation is performed based on a thresholding (200 [HU]) followed by morphological operations (opening, radius = 3.0 [mm]) and a hole filling process.

Third process is a rough extraction of the liver using a thresholding (300[HU]). The two connected components with the largest volumes are defined and forwarded to the human specific shape estimation process as well as to the fine liver segmentation process where the components are used as object seeds in graph cuts. Here all these parameters, such as threshold values, filter sizes as well as parameters in the following process were decided experimentally using training data.

The fourth process is body cavity extraction, which is used to place landmarks for the registration of the SSM of the liver and aorta, as well as neighbor constraint, NB_b, for fine liver segmentation. The registration process for the SSM of liver and aorta uses landmarks placed on the abdominal organ. First, we obtain the top and bottom slices of a rough segmentation of the liver and find the four slices that are spatially uniformly distributed between the top and bottom slices. Landmarks are then automatically placed on the six slices and on the topmost point in each slice. In order to register an SSM to an input image, we used the average position of the landmarks from the training data.

The rough segmentation results might seem to be inaccurate. It is, however, accurate enough to place landmarks reliably. The most of the segmentation error of the rough segmentation came from false negatives must be enhanced. The next process is aorta segmentation, which provides neighbor prior information and uses a single-shape graph cut with the following energy function.

ISSN (ONLINE): 2454-9762
ISSN (PRINT): 2454-9762

International Journal of Advanced Research in Management, Architecture, Technology and Engineering (IJARMATE)
Vol. 2, Issue 10, October 2016

$$E(A) = \lambda . \sum_{p \in P} \{R_{aorta(p)}\ (A_p)\ Atlus_{\ p}(A_p)\} + \sum_{\{p,q\} \in n} \{B_{p,q} + S_{p,q}\} . \delta A_p \neq A_q$$

where F_p represents a feature vector based on the intensity value at voxel p and $R_{aorta(p)}\ (A_p)$ is defined by posterior probabilities of aorta and other, both of which are computed from likelihood functions estimated by Parzen window estimator and uniform prior probabilities. $Atlas_{\ p}(A_p)$ is a prior probability of the aorta computed from training data. A registered shape template of an aorta from training data is used as the shape prior of $S_{p,q}$.

The next process is the estimation of human-specific shapes. Calculate a Jaccard index (JI) as a metric to compute the distance between a rough segmented region and the shapes in an eigen shape space. Here, we employed a level set distribution model (LSDM) [12] with a weighted principal component analysis (WPCA) [13] used as a statistical analysis method to construct the eigen shape space of a SSM, which has proved effective in modeling an organ's shape

The rough segmentation result is projected to the eigen space spanned by the first two eigen modes and the closest shape to the rough segmentation is selected from among 25 shapes in the eigen shape space. In the multi-shape graph cuts, the top five closest shapes in terms of JI are chosen. The 25 shapes are generated by discretizing the eigen-shape space with 1^{σ} spacing from the projection point with a range of $\pm 2^{\sigma}$.

The final process is fine liver segmentation by the multi-shape graph cuts which is discussed in preceding section.

This subsection presents a graph cut-based segmentation algorithm that can solve the problem encountered when multiple shape priors are combined. Unlike conventional graph cut algorithms, which deal with binary label problems, now consider multiple-shape priors, or multiple labels. Let a set, L, be a label set {0, 1, 2,..., n} in which each label corresponds to a prior shape. The goal is to develop an algorithm that will select an optimal shape prior at each voxel by minimizing the energy function, including the shape energy equation shown below.

$$E_{shape} = \sum_{\{p,q\} \in n} S_{p,q} . \delta$$

$$S_{p,q} = MIN \left(\sqrt{\frac{1-\cos(\theta A_p)}{2}}, \sqrt{\frac{1-\cos(\theta A_q)}{2}} \right)$$

where θA_p represents the angle between a vector connecting voxels p and q, and a gradient vector of a signed distance $\varphi A_p(p)$ from the boundary of a shape corresponding to a label. $A_p \in L.$ Here, δ is a function that equals 0 when the neighboring voxels belong to the same class and 1 otherwise.

Ideally, it is best to solve a multi-label problem in one step. When labels in a set L have certain relationships to each other, such as containment and attraction relationships, there are algorithms that guarantee a global optimum of the multi-label problem [14] However, when labels do not have such relationships, as in our case, there is no algorithm that can handle problems in this manner. An important drawback of this algorithm [14] is that the fusion move algorithm can simultaneously propose multiple labels in varying locations, but the alpha-expansion algorithm cannot.

Multi-shape GC algorithm proposes labels that differ by location so as to ensure the sub-modularity of the shape energy. Consequently, the fusion move algorithm is employed which iteratively solves a series of problems between a set of current labels and a set of proposed labels using the QPBO (Quadratic Pseudo-Boolean Optimization) min-cut algorithm.

The QPBO min-cut algorithm can find a combinatorial optimal solution of labels, or shapes as its first step called as object labels. This step can reduce false negatives, but cannot deal with false positives. The second step, background labels focuses on false positives based on the same analogy.

To differentiate between background labels and object labels, negative labels are introduced to represent back-ground labels. An iterate a pair of object and background proposals by changing a label, or a prior shape. The algorithm stops the iteration process when no label changes or when it reaches the maximum number of iterations defined by the user.

The final energy used for the proposed method, neighbor constrained multi-shape graph cuts, is given in Eq. (3.17), in which a probabilistic atlas-based data term, $Atlas_{\ p}(A_p)$ is combined with the energies outlined in Sections 3.5.1.2.

$$E(A) = \sum_{p \in P} \lambda . NB(p). \{R_p\ (A_p) + Atlas_p\ (A_p)\} + NB_p\ (A_p) + \sum_{\{p,q\} \in n} \{B_{p,q} + S_{p,q}\} . \delta_{A_p, A_q < 0}\ \delta_{NBbp} = NBP_q$$

Thus the multi-shape Graph Cut technique is used to delineate the image from an abdominal organ. This proposed technique is reducing the delineation time factor than the existing method used in phase I. This time factor is shown in the chapter 4 result part.

The performance of GC-OAAM method is improved based on multiple MTANN. Some advanced CAD schemes employ a filter for enhancement of lesions as a preprocessing step for improving sensitivity and specificity. The filter enhances objects similar to a model employed in the filter;

ISSN (ONLINE): 2454-9762
ISSN (PRINT): 2454-9762

International Journal of Advanced Research in Management, Architecture, Technology and Engineering (IJARMATE)
Vol. 2, Issue 10, October 2016

e.g., a blob enhancement filter based on the Hessian matrix enhances sphere-like objects [15]. The conventional filters often fail to enhance actual lesions such as lung nodules with ground-glass opacity and sessile/flat polyps. To address this issue, we developed a supervised filter for enhancement of actual lesions by use of a massive-training artificial neural network (MTANN) [16] filter in a CAD scheme.

A computer-aided detection (CADe) scheme [19], [20] for nodules in chest or abdominal radiographs (CXR) has been investigated for assisting radiologists in improving their sensitivity. Although a great deal of work has been done by researchers to improve the performance of CADe schemes, CADe schemes still produce a relatively large number of false positives (FPs). This would distract radiologists in their detection and reduce radiologists' efficiency. In addition, radiologists may lose their confidence with the CADe scheme as a useful tool.

Matsumotoet al. conducted observer studies [21], which showed that, if a CADe scheme had a high FP rate of 11 per image, radiologists' accuracy in detecting nodules was not improved when they were aided by computer output, even though the scheme had a high sensitivity of 80%. Radiologists' accuracy, however, was significantly improved if the CADe scheme had a simulated low FP rate with the same sensitivity. Therefore, having a low FP rate is critical for a CADe scheme to be useful. A number of investigators developed FP reduction methods [21]–[23].

Yoshidaet al. proposed a method called local contra lateral subtraction to remove normal anatomic structures in CXRs based on the symmetry between the left and right lung regions for FP reduction [11]. Suzuki et al. developed a multiple massive-training artificial neural networks (MTANNs) to reduce the number of FPs produced by their CADe scheme [12]. Loog et al. investigates if the conspicuity of lung nodules increases when applying the suppression technique in CXR. Other abnormalities may also be detected, classified, and quantified more accurately if the bony anatomy is adequately suppressed [14].

To enhance actual lesions in medical images, developed an MTANN unsupervised filter. The architecture of an MTANN supervised filter is shown in Fig. 1. An MTANN filter consists of a linear-output regression artificial neural network (LOR-ANN) model [17], which is a regression-type ANN capable of operating on pixel/voxel data directly.

The MTANN filter is trained with input CT or MRI images and the corresponding "teaching" images that contain a map for the "likelihood of being lesions." The pixel values of the input images are linearly scaled such that –1,000 Hounsfield units (HU) correspond to 0 and 1,000 HU corresponds to 1. The input to the MTANN filter consists of pixel values in a sub-region, R_s, extracted from an input image.

The output of the MTANN filter is a continuous scalar value, which is associated with the center pixel in the sub-region, and is represented by

$$O(x,y) = LOR - ANN\{ I(x-i),(y-j)|(i,j)R_s$$

where x and yare the coordinate indices, LOR-ANN (·) is the output of the LOR-ANN model, and I(x, y) is a pixel value in the input image.

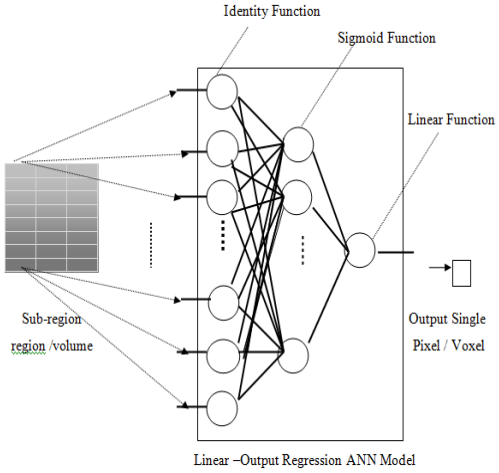

Fig.2.Architecture of an MTANN supervised filter

The architecture of an MTANN supervised filter consisting of a LOR-ANN model with sub-region input and single-pixel output. All pixel values in a sub-region extracted from an input CT image. The LOR-ANN output is a single pixel value for each sub-region, the location of which corresponds to the center pixel in the sub-region. Output pixel value is mapped back to the corresponding pixel in the output image.

To create the teaching image, lesions are segmented manually for obtaining a binary image with 1 being lesion pixels and 0 being non-lesion pixels. Then, Gaussian smoothing is applied to the binary image for smoothing down the edges of the segmented lesions, because the boundary of the lesion likelihood of being lesions should gradually is diminished as the distance from decreases. Note that the ANN was not able to be trained when binary teaching images were used.

The MTANN filter involves training with a large number of pairs of sub-regions and pixels; it is called as a massive-sub-region training scheme. For enrichment of the training samples, a training image, RT, extracted from the input CT or MRI image is divided pixel by pixel into a large number of sub-regions. Note that close sub-regions overlap each other. Single pixels are extracted from the corresponding teaching image as teaching values. The MTANN filter is massively trained by use of each of a large number of input sub-regions together with each of the corresponding teaching single pixels; hence the term "massive-training ANN."

The MTANN filter is trained by a linear-output back-propagation (BP) algorithm where the generalized delta rule [18] is applied to the LOR-ANN architecture [17]. After

ISSN (ONLINE): 2454-9762
ISSN (PRINT): 2454-9762

International Journal of Advanced Research in Management, Architecture, Technology and Engineering (IJARMATE)
Vol. 2, Issue 10, October 2016

training, the MTANN filter is expected to output the highest value when a lesion is located at the center of the sub-region of the MTANN filter, a lower value as the distance from the sub-region center increases, and zero when the input sub-region contains a non-lesion.

The input CT image or MRI is divided pixel by pixel into a large number of overlapping sub-regions. The corresponding pixels are extracted from the "teaching" image containing a map for the "likelihood of being a lesion." The MTANN filter is trained with pairs of the input sub-regions and the corresponding teaching pixels. Scanning with the trained MTANN filter is performed for obtaining pixel values in the entire output image.

In order to distinguish malignant nodules from various types of benign nodules, we extended the capability of a single MTANN and developed multiple MTANNs (multi-MTANN) [25]. The multi-MTANN consists of plural MTANNs that are arranged in parallel. Each MTANN is trained by use of benign nodules representing a different benign type, but with the same malignant nodules.

Each MTANN acts as an expert for distinguishing malignant nodules from a specific type of benign nodule, e.g., MTANN no.1 is trained to distinguish malignant nodules from small benign nodules overlapping with vessels; MTANN no. 2 is trained to distinguish malignant nodules from medium-sized benign nodules with fuzzy edges; and so on.

Liver in abdomen radiographs include various spatial-frequency components. For a single MTANN, suppression of ribs containing such various frequencies is difficult, because the capability of a single MTANN is limited, i.e., the capability depends on the size of the sub-region of the MTANN. Because the training of the MTANN takes a substantially long time, it is difficult in practice to train the MTANN with a large sub-region.

In order to overcome this issue, multi resolution decomposition/composition techniques are employed. The multi resolution decomposition is a technique for decomposing an original high-resolution image into different-resolution images.

First, one obtains a medium-resolution image $g_M(x, y)$ from an original high-resolution image by $g_H(x, y)$ performing down-sampling with averaging, i.e., four pixels in the original image are replaced by a pixel having the mean value for the four pixel values, represented by

$$g_M(x, y) = \frac{1}{4}\sum_{i,j \in R_{22}} g_H(2x - i, 2y - j)$$

where R_{22} is a 2-by-2-pixel region. The medium-resolution image is enlarged by up-sampling with pixel substitution, i.e., a pixel in the medium-resolution image is replaced by four pixels with the same pixel value, as follows:

$$g_M^U(x, y) = g_M\left(\frac{x}{2}, \frac{y}{2}\right)$$

Then, a high-resolution difference image $d_H(x, y)$ is obtained by subtraction of the enlarged medium-resolution image from the high-resolution image, represented by

$$d_H(x, y) = g_M(x, y) - g_M^U(x, y)$$

These procedures are performed repeatedly, producing further lower-resolution images. Thus, multi resolution images having various frequencies are obtained by use of the multi resolution decomposition technique.

An important property of this technique is that exactly the same original-resolution image $g_H(x, y)$ can be obtained from the multi resolution images $d_H(x, y)$ and $g_M(x, y)$, by performing the inverse procedures, called a multi resolution composition technique as follows:

$$g_H(x, y) = g_M\left(\frac{x}{2}, \frac{y}{2}\right) + d_H(x, y)$$

Therefore, multi resolution images can be processed independently instead of processing original high-resolution images directly; i.e., with these techniques, the processed original high-resolution image can be obtained by composing of the processed multi resolution images.

An MTANN only needs to support a limited spatial frequency rage in each resolution image instead of the entire spatial frequencies in the original image. Therefore, multiple MTANN technique would be potentially useful for radiologists to detect false positives as well as for CAD schemes in the detection of lung nodules in chest radiograph.

IV. RESULTS AND DISCUSSION

The statistical measures such as FPR, TRR, ACC, PPV and MCC are calculated. These values are shown as graphical representations. The graphs are shown as a screen shot.

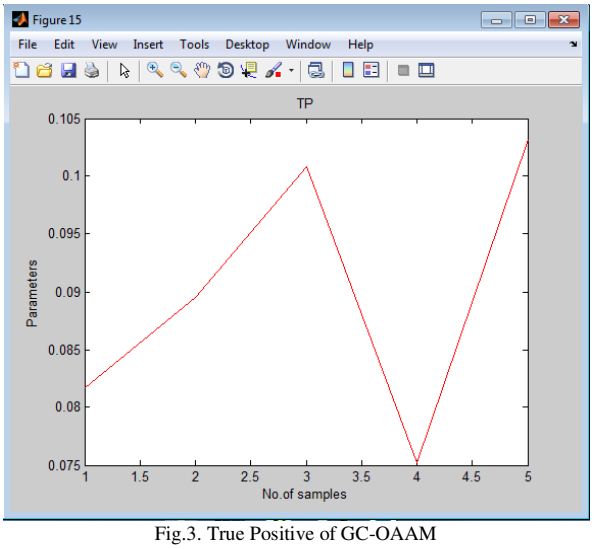

Fig.3. True Positive of GC-OAAM

ISSN (ONLINE): 2454-9762
ISSN (PRINT): 2454-9762

International Journal of Advanced Research in Management, Architecture, Technology and Engineering (IJARMATE)
Vol. 2, Issue 10, October 2016

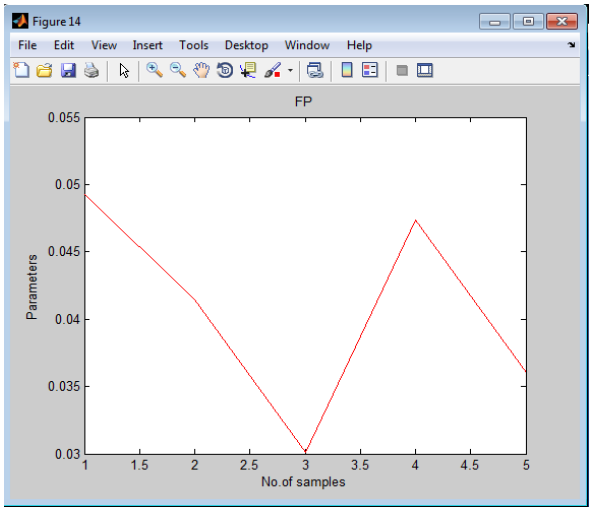

Fig.4. False Positive of GC-OAAM

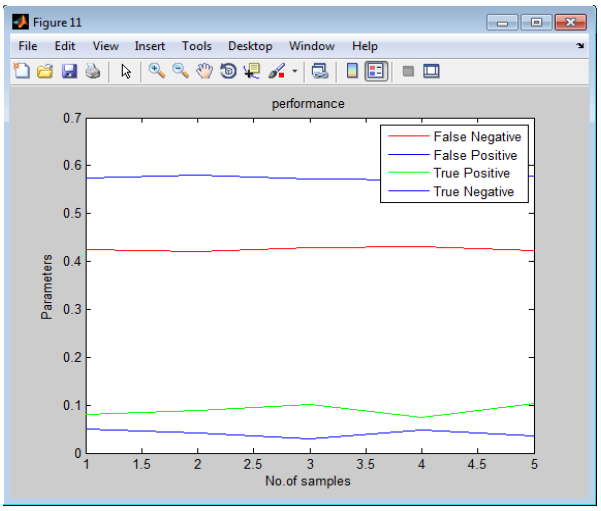

Fig.7. Performance of GC-OAAM

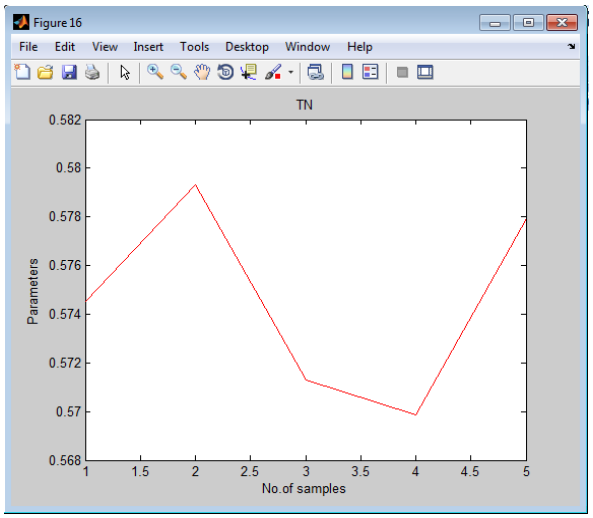

Fig.5. True Negative of GC-OAAM

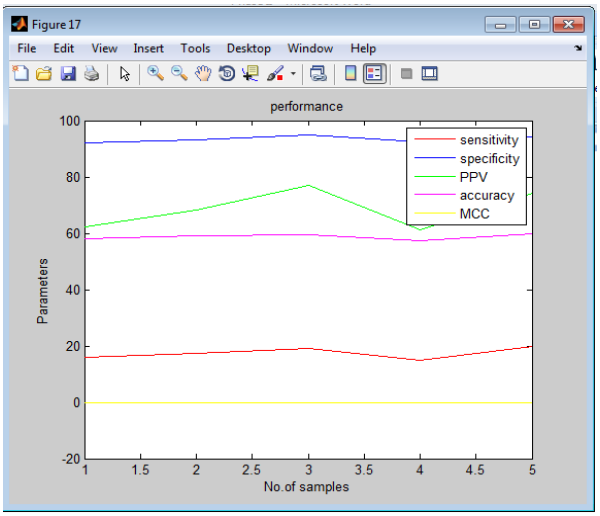

Fig.9. Comparative Performance of GC-OAAM

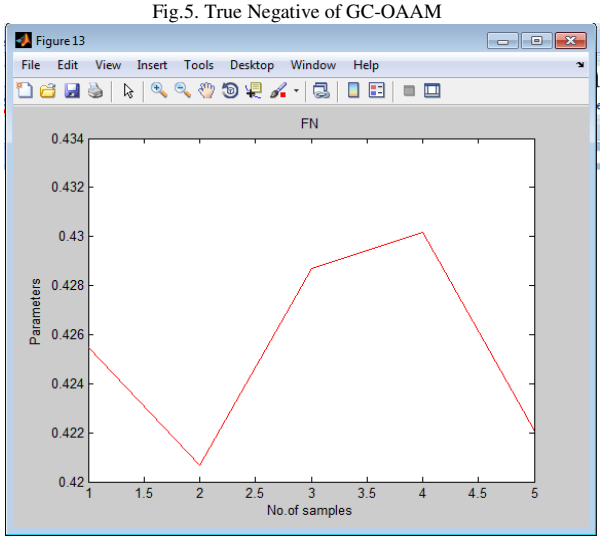

Fig.6. False Negative of GC-OAAM

The segmentation results that are obtained from MTANN are compared with the ground truth images.

These statistical measures such as FPR, TRR, ACC, PPV and MCC are calculated. These values are shown as graphical representations. The graphs are shown as a screen shot.

ISSN (ONLINE): 2454-9762
ISSN (PRINT): 2454-9762

International Journal of Advanced Research in Management, Architecture, Technology and Engineering (IJARMATE)
Vol. 2, Issue 10, October 2016

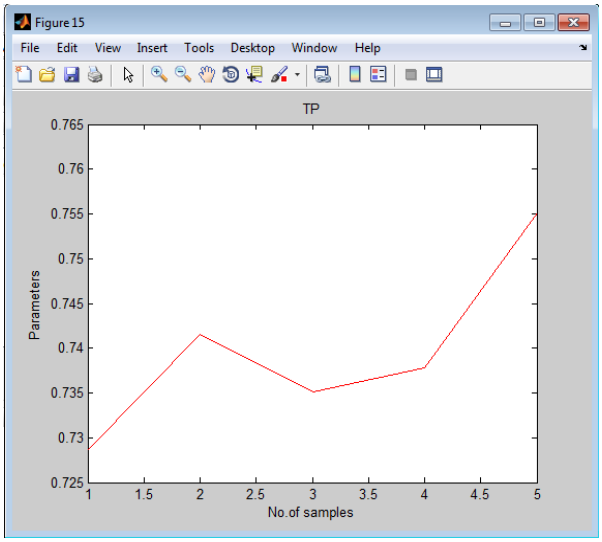

Fig. 10. True Positive of MTANN Output

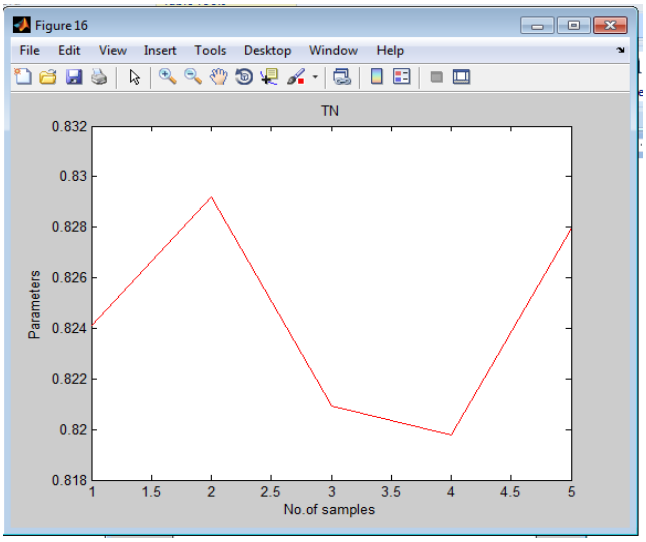

Fig.12. True Negative of MTANN Output

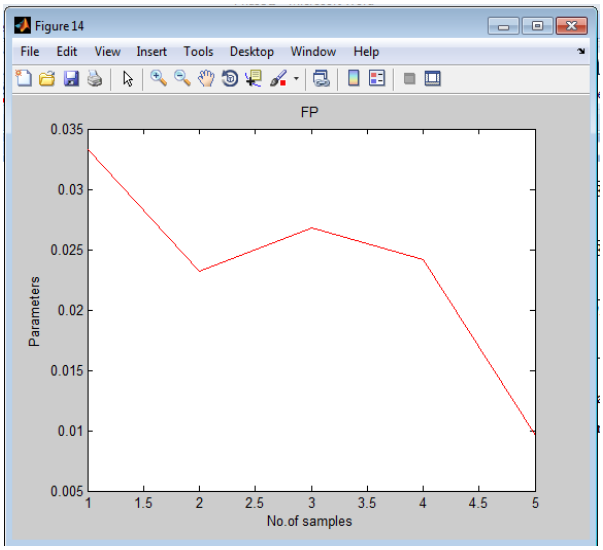

Fig.11. False Positive of MTANN Output

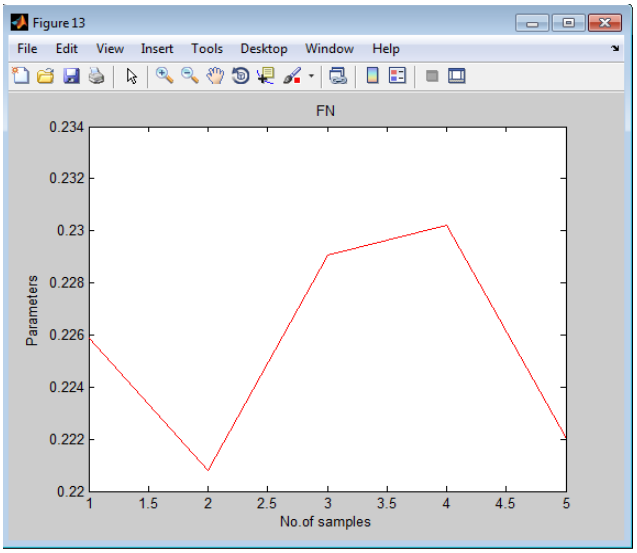

Fig.13. False Negative of MTANN Output

ISSN (ONLINE): 2454-9762
ISSN (PRINT): 2454-9762

International Journal of Advanced Research in Management, Architecture, Technology and Engineering (IJARMATE)
Vol. 2, Issue 10, October 2016

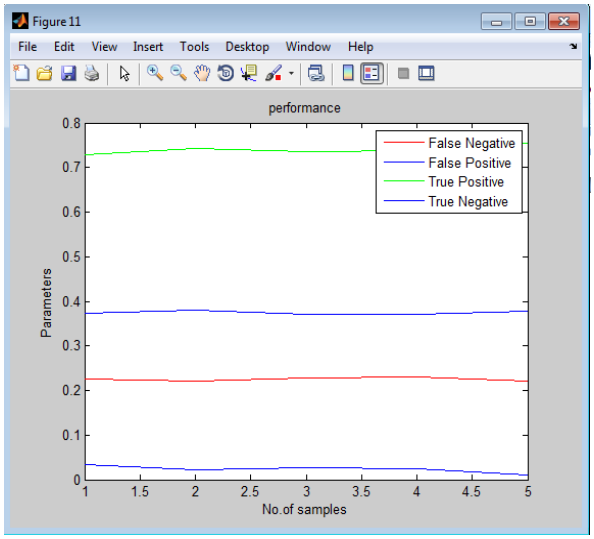

Fig.14. Performance of MTANN Output

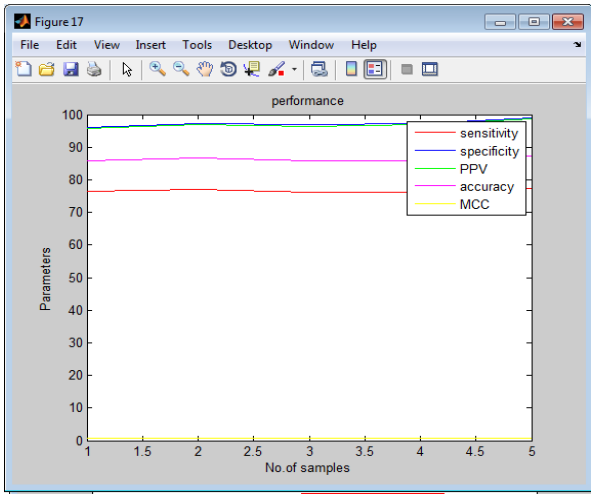

Fig.15. Comparative Performance of MTANN Output

V. CONCLUSION

Adaptive initialization method allows a fully automatic liver and tumors segmentation employing active contour or graph-cut based techniques. MATLAB 7.11.0 (R 2010b) tool is used to implement this proposed work. This study presented the implementation of two fully automatic liver and tumors segmentation techniques and their comparative assessment. Image segmentation plays a crucial role in many medical-imaging applications, by automating or facilitating the delineation of anatomical structures and other regions of interest. Many methods are existing and still developing the new methods for the segmentation to overcome the shortcomings of the existing methods. The liver image is segmented by using GC-OAAM approach in Phase I. This segmentation work is analyzed by using confusion algorithm. The performance is improved by the implementation of multiple MTANN. The MTANN supervised filter was effective for enhancement in medical images and is useful for improving the sensitivity and specificity. The described adaptive initialization method enabled fully automatic liver surface segmentation with both Geodesic Graph Cut and Graph-Cut techniques, demonstrating the feasibility of two different approaches. The comparative assessment showed that the Geodesic Graph-cut method provided superior results in terms of accuracy and did not present the described main limitations related to the Graph Cut method. In the previous work, the initialization technique was applied to Graph Cuts algorithm demonstrating the robustness and effectiveness of automatic liver segmentation.

In this study, the initialization method was further extended to Geodesic Graph cut algorithm in order to enable full automation of this method and evaluate potential improvements with respect to previous automatic presented approaches and then to the ground truth. The same segmentation approaches were then applied also to segmentation of liver tumors. Even if there are some theoretical connections between discrete geometry of Geodesic Graph-cuts and integral and differential geometry related to Graph Cuts approach, important differences cannot be neglected for algorithm implementations and comparative assessment of the results.

REFERENCES

[1] Yalcina.B., Richterc.G., Krausb.T., Büchlerb.M.W and Thorna.M.(2004) "Computer-based surgery planning for living liver donation," Int Arch. Photogram Rem. Sens. Spatial Inform. Sci., vol.35, pp. 291–295.

[2] Yushkevich.P.A. (2006) "User-guided 3D active contour segmentation of anatomical structures: Significantly improved efficiency and reliability," Neuroimage, vol. 31, pp. 1116–1128, Jul. 2006.

[3] Zhao.B., Kijewski.P.K., Wang.L., and Schwartz.L.H.(2005) "Liver segmentation for CT images using GVF snake," Med. Phys., vol. 32, pp. 3699–3706.

[4] Zientkowska.M., Domeyer-Missbach.M. (2008) "Morphologic changes of mammary carcinomas in mice over time as monitored by flat-panel detector volume computed tomography," Neoplasia, vol. 10, pp. 663–673.

[5] Zuna.J. and Schlegel.W. (2000) Usability of semiautomatic segmentation algorithm for tumor volume determination," Invest. Radiol., vol. 34, pp. 143–150.

[6] A. Ayvaci and D. Freedman, "Joint segmentation-registration of organs using geometricmodels," in Proc. IEEE Eng.Med. Biol. Soc., 2007,pp. 5251–5254.

[7] R. Anderson and J. Setubal, "A parallel implementation of the pushrelabel algorithm for the maximum flow problem," J. Parallel Distrib. Comput., vol. 29, no. 1, pp. 17–26, Aug. 1995.

[8] A. Besbes, N. Komodakis, G. Langs, and N. Paragios, "Shape priors and discrete MRFs for knowledge-based

ISSN (ONLINE): 2454-9762
ISSN (PRINT): 2454-9762

International Journal of Advanced Research in Management, Architecture, Technology and Engineering (IJARMATE)
Vol. 2, Issue 10, October 2016

segmentation," in Proc.IEEE Comput. Soc. Conf. Comput. Vis. Pattern Recogn., 2009, pp. 1295–1302.
[9] Y. Boykov and V. Kolmogorov, "An experimental comparison of mincut/ max-flow algorithms," IEEE Trans. Pattern Anal. Mach. Intell., vol. 26, no. 9, pp. 1124–1137, Sep. 2004.
[10] Y. Boykov, O. Veksler, and R. Zabih, "Fast approximate energy minimization via graph cuts," IEEE Trans. Pattern Anal. Mach. Intell., vol. 23, no. 11, pp. 1222–1239, Nov. 2001.
[11] T. F. Cootes, G. Edwards, and C. Taylor, "Active appearance models," IEEE Trans. Pattern Anal. Mach. Intell., vol. 23, no. 6, pp. 681–685, Jun. 2001.
[12] T. F. Cootes, C. J. Taylor, D. H. Cooper, and J. Graham, "Active shape models—Their training and application," Comput. Vis. Image Underst., vol. 61, no. 1, pp. 38–59, Jan. 1995.
[13] T. Emrich, F. Graf, H. P. Kriegel, M. Schubert, M. Thoma, and A. Cavallaro, "CT slice localization via instance-based regression," in Proc.SPIE, 2010, vol. 7623, pp. 762 320-1–762 320-12.
[14] A. X. Falcao, J. K. Udupa, S. Samarasekera, and S. Sharma, "User-steered image segmentation paradigms: Live wire and live lane," Graph. Models Image Process., vol. 60, no. 4, pp. 233–260, Jul.1998.
[15] D. Freedman and T. Zhang, "Interactive graph cut based segmentation with shape priors," in Proc. IEEE Comput. Soc. Conf. Comput. Vis.Pattern Recogn., 2005, pp. 755–762.
[16] B.Haas, T. Coradi, M. Scholz, P.Kunz,M.Huber,U.Oppitz, L.André,V.Lengkeek, D. Huyskens, A. van Esch, and R. Reddick, "Automatic segmentation of thoracic and pelvic CT images for radiotherapy planning using implicit anatomic knowledge and organ-specific segmentation strategies," Phys. Med. Biol., vol. 53, no. 6, pp. 1751–1771, Mar.2008.